Natural Resources for Human Health

eISSN: 2583-1194

Original Research

Received 20 May 2026
Revised 30 June 2026
Accepted 14 July 2026

Natural Resources for Human Health 2026, Vol. 6(7s): 1224–1243

KEYWORDS:
Planomicrobium sp. A9, organophosphate hydrolase, TCP metabolite, chromium (VI) biodetoxification, esterase, indigenous bioremediation, oxidative stress

Organophosphate Hydrolase-Mediated Chlorpyrifos Transformation and Chromium Biodetoxification by Indigenous Planomicrobium sp. A9 From Co-Contaminated Haryana Soils: Enzyme Confirmation, TCP Metabolite Tracking and Oxidative-Stress Characterization

Anjali Phogat[1], Tanvi Singh[1], Rajendra Prasad[1], Atanu Banerjee[1], Sangeeta Gohel[2], Sangeeta Kumari[1*]

[1]Amity Institute of Biotechnology, Amity University Haryana, Gurugram, 122413, India
[2]Department of Biosciences, Saurashtra University, Rajkot, Gujarat-360005, India
Email- ID: anjaliphogat0@gmail.com, aks.tanvi28@gmail.com, sdgohel@sauuni.ac.in, rprasad@ggn.amity.edu, abanerjee1@ggn.amity.edu, sanshnic@gmail.com
*Corresponding Author: Sangeeta Kumari (sanshnic@gmail.com)

ABSTRACT: Co-contaminated soils bearing simultaneous heavy metal and organophosphate pesticide loads present a toxicological complexity that single-contaminant bioremediation frameworks cannot adequately address. This study applies a two-block evidence framework to *Planomicrobium sp.* A9, an indigenous isolate from industrially co-contaminated soils of Haryana, India. The first block quantifies the oxidative-stress response: malondialdehyde reached 58.27 μmol mg^{-1} protein, while SOD inhibition (3.91%), catalase activity (k = 0.040 s^{-1} mL^{-1}) and reduced glutathione (0.4 nM mg^{-1} protein) were measurable but low, consistent with partial antioxidant depletion under chronic multi-contaminant stress. The second block provides direct transformation evidence: OPH/phosphotriesterase specific activity of 0.045 U mg^{-1} protein (44.7-fold above heat-inactivated control) and esterase activity of 0.155 U mg^{-1} protein (8.6-fold above control) confirms enzyme-linked organophosphate bond cleavage. Targeted GC-MS monitoring of chlorpyrifos and its primary metabolite TCP showed transient accumulation peaking at 2.74 mg L^{-1} at 24 h before declining to 0.16 mg L^{-1} by 72 h, kinetically distinguishing active enzymatic hydrolysis from abiotic loss. A diphenylcarbazide colorimetric assay confirmed 69.2% Cr(VI) reduction within 48 h, independently corroborating ICP-MS total chromium data (68.09%) from the companion study. KEGG pathway analysis contextualized TCP kinetics within the documented OPH-initiated hydrolytic route. Six convergent evidence layers establish *Planomicrobium sp.* A9 as an enzymatically competent, multi-stress-adapted candidate for bioremediation of mixed heavy metal–pesticide environments, constituting, to our knowledge, the first enzyme-level and metabolite-tracking characterization of this bacterial isolate under authentic industrial co-contamination conditions.

HIGHLIGHTS

- A9 (*Planomicrobium* sp.) isolated from co-contaminated industrial soils, Haryana
- OPH 44.7-fold above heat-inactivated control; specific activity 0.045 U/mg

Natural Resources for Human Health
eISSN: 2583-1194

- TCP peak at 24 h proves enzymatic chlorpyrifos hydrolysis over adsorption
- Cr(VI) reduction 69.2% by live A9; ICP-MS and DPC converge within 1.1%
- MDA high, SOD depleted, GSH near-zero: chronic co-stress adaptation confirmed

Graphical Abstract

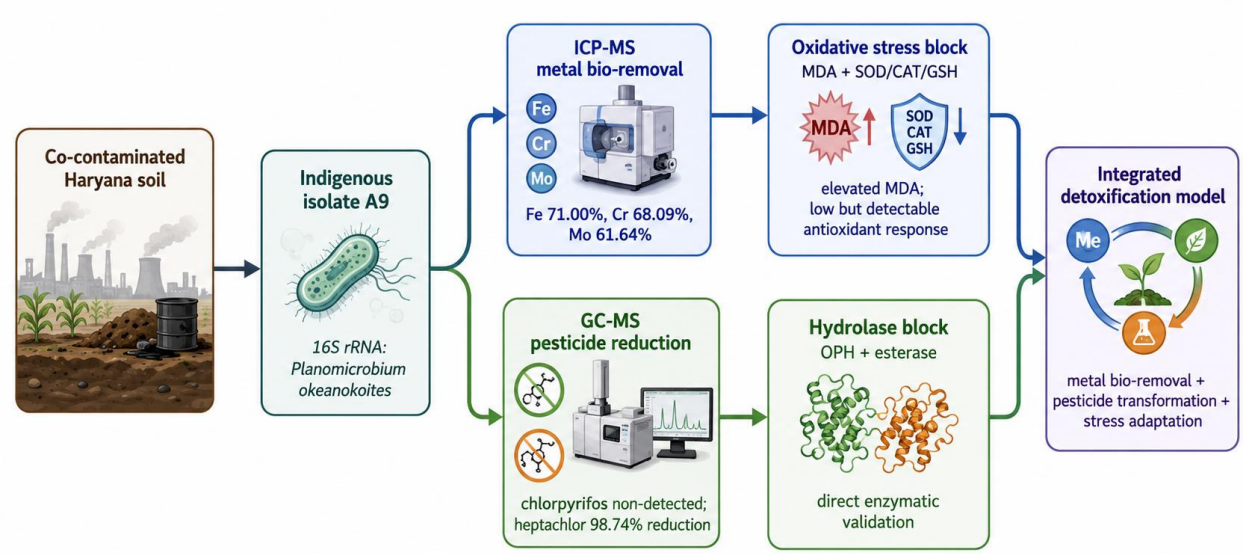

1. INTRODUCTION

Haryana's peri-urban industrial belt has become a pronounced example of multi-contaminant soil degradation. Foundry emissions, electroplating effluent and agricultural runoff simultaneously deposit iron, chromium, molybdenum and lead into surface soils where repeated application of organophosphate pesticides, chlorpyrifos in particular, has been standard agricultural practice for decades (Zhang et al., 2020; Pegu et al., 2025; Li et al., 2025). The combined metal toxicity and xenobiotic enzyme inhibition this creates is substantially more damaging to indigenous microbial communities than either stressor alone, yet it also selects, over ecologically relevant timescales, for organisms capable of operating under both (Gadd, 2010; Haque et al., 2021; Ayub et al., 2025).

Among the metals of concern, Cr(VI) is particularly hazardous — soluble, membrane-permeable and acutely genotoxic. Its biological reduction to Cr(III) constitutes genuine detoxification rather than mere removal from solution (Pande et al., 2022). Iron and molybdenum at elevated dissolved concentrations disrupt soil enzyme activity and plant nutrition, but ICP-MS bulk removal figures alone cannot distinguish biosorption, precipitation or intracellular sequestration as the operative mechanism (Zhang et al., 2020; Zhou et al., 2023). This mechanistic ambiguity motivates the complementary use of speciation-specific assays alongside bulk removal data.

Chlorpyrifos adds its own interpretive complication. Its primary hydrolysis product, 3,5,6-trichloro-2-pyridinol (TCP), accumulates in aerobic soils and carries an independent ecotoxicological profile that can exceed that of the parent compound (Bose et al., 2021; Adams et al., 2024; Batool et al., 2023). Endpoint GC-MS non-detection of chlorpyrifos cannot rule out adsorption, abiotic hydrolysis or analytical matrix suppression, making targeted metabolite monitoring an essential complement to residue-reduction reporting (Mali et al., 2022). The enzyme primarily responsible for the initial P–O–C bond cleavage is organophosphate hydrolase (OPH)/phosphotriesterase; its quantification in crude extracts has been validated in benchmark strains including *Pseudomonas nitroreducens* AR-3 and *Cupriavidus nantongensis* X1T (Aswathi et al., 2019; Fang et al., 2021).

Planomicrobium sp. A9, most closely related to *P. okeanokoites* NBRC 12536 (97.71% 16S rRNA similarity) *(family Planococcaceae, order Bacillales)* is a motile, pigmented, Gram-positive organism first isolated from marine environments (Yoon et al., 2001). Its

representation in terrestrial heavy metal–pesticide bioremediation literature is minimal (Saini et al., 2023), and no published study has evaluated a *Planomicrobium* isolate under combined co-stress using enzyme-level confirmation, targeted metabolite monitoring and Cr(VI) speciation. Its Gram-positive cell envelope, with carboxylate, hydroxyl and phosphate surface groups, is structurally well-suited to metal chelation; its recovery from chronically co-contaminated Haryana soils implies ecologically relevant multi-stress adaptation.

This manuscript and the companion study (Phogat et al., under review) form a planned two-part series with complementary and non-overlapping evidence scopes. The companion paper establishes ICP-MS-based heavy metal bio-removal and GC-MS pesticide residue reduction as the primary chemical evidence layer; the present study provides the mechanistic layer — quantitative enzyme assays, targeted metabolite kinetics, Cr(VI) speciation colorimetry and oxidative-stress biomarker quantification — that the companion paper explicitly identified as requiring separate detailed reporting. Each manuscript is independently interpretable in scope and contribution, and the two together constitute the full evidence framework for *Planomicrobium sp.* A9.

The two-block framework applied here is intentionally conservative: Block I (physiological) uses MDA, SOD, catalase and GSH to characterize oxidative-stress adaptation without conflating antioxidant responses with pesticide degradation. Block II (transformation) uses OPH and esterase activities, TCP metabolite kinetics and Cr(VI) colorimetry for direct mechanistic evidence. The objectives were: (i) to quantify OPH and esterase activities in A9 crude extracts; (ii) to track TCP alongside chlorpyrifos over 72 h by targeted GC-MS; (iii) to confirm Cr(VI) reduction by diphenylcarbazide colorimetry; (iv) to characterize oxidative-stress biomarkers; and (v) to integrate results with KEGG pathway bioinformatics and comparative literature analysis.

2. MATERIALS AND METHODS

2.1 Bacterial isolate and culture conditions

Isolate A9, identified as *Planomicrobium sp.* A9, most closely related to *P. okeanokoites* NBRC 12536 (97.71% 16S rRNA similarity) (97.71% 16S rRNA similarity) in the companion study (Phogat et al., under review), was recovered from co-contaminated industrial-agricultural soils at Rohtak, Gurugram and Bahadurgarh (Haryana, India). Sites were characterized by mixed inputs from foundry effluent, electroplating discharge, agricultural runoff and municipal sludge. Samples were collected from 0–15 cm depth. Stock cultures were maintained on nutrient agar at 28 °C; overnight nutrient broth cultures (37 °C, 150 rpm) served as inoculum for all assays.

2.2 Molecular identification

Complete 16S rRNA sequencing, BLASTn identity confirmation, neighbour-joining phylogenetic tree construction in MEGA X (Kumar et al., 2015) and species assignment at the 97% similarity threshold (Yarza et al., 2014) are reported in full in the companion study (Phogat et al., under review). The 16S rRNA gene sequence of isolate A9 has been deposited in NCBI GenBank under accession number PZ625846.

2.3 Co-contaminant stress exposure

For oxidative-stress assays, A9 cultures were exposed to a multi-metal mixture ($FeCl_3$, $CrCl_3$ and Na_2MoO_4; each 500-µg L^{-1}) combined with chlorpyrifos (10 mg L^{-1}) in nutrient broth for 48 h at 30 °C, 150 rpm, alongside unexposed controls. Concentrations reflected environmentally relevant co-contamination levels reported for Haryana industrial soils (Zhang *et al.*, 2020; Li *et al.*, 2025).

2.4 Crude extract preparation and protein quantification

Cells were harvested at 8,000 × g (10 min, 4 °C), washed twice with 50 mM phosphate buffer (pH 7.0), resuspended and sonicated (3 × 30 s pulses, 4 °C). Lysates were clarified at 10,000 × g (15 min) and the supernatant used for all enzyme assays. Protein was quantified by the Bradford dye-binding method with BSA as standard (Bradford, 1976).

2.5 Superoxide dismutase (SOD)

SOD activity was measured using the xanthine/xanthine oxidase (XO) photochemical NBT inhibition method (Beauchamp and Fridovich, 1971). Superoxide radicals generated in situ by the XO system reduce NBT; SOD present in the sample inhibits this reduction. Absorbance was monitored at 560 nm. Activity was expressed as percentage inhibition of NBT

reduction, calculated as: Inhibition (%) = [(Control XO rate − Sample rate) / Control XO rate] × 100. Measurements were made at a 1:1 dilution of crude extract under the stated assay conditions.

2.6 Catalase (CAT)

Catalase activity was measured by monitoring the first-order decomposition of H_2O_2 at 240 nm (Aebi, 1984). The reaction contained 50 mM phosphate buffer (pH 7.0) and 10 mM H_2O_2; absorbance was recorded for 2 min at 25 °C. The first-order rate constant was calculated as: $k = (1/60) \times \ln(A_0/A_{60})$, where A_0 and A_{60} are absorbance at 0 and 60 s respectively. Total catalase activity per milliliter of extract was normalized as: $k\_total\ mL^{-1} = k \times (6 / \text{sample volume in mL})$. Results are expressed as $s^{-1}\ mL^{-1}$.

2.7 Reduced glutathione (GSH)

Reduced glutathione was quantified by the kinetic recycling method (Tietze, 1969) in a 96-well microplate format. GSH is continuously recycled by glutathione reductase (GR) in the presence of β-NADPH; the concomitant reduction of 5,5'-dithio-bis-(2-nitrobenzoic acid) (DTNB) to 2-nitro-5-thiobenzoic acid (TNB) was monitored at 412 nm over five time points. Total GSH concentration was calculated as: GSH = (Slope_sample − Slope_blank) / Slope_standard, where slopes were derived from linear regression of absorbance versus time. Results are expressed as nM mg^{-1} protein.

2.8 Malondialdehyde (MDA) - lipid peroxidation

Lipid peroxidation was estimated by the thiobarbituric acid (TBA) reactive substances method (Ohkawa et al., 1979). Crude extracts were combined with SDS (8.1% w/v), 20% glacial acetic acid and 0.8% TBA solution, then incubated at 100 °C for 60 min. After centrifugation (8,000 rpm, 10 min), absorbance was measured at 532 nm. MDA concentration was determined from a 1,1,3,3-tetraethoxypropane (TMP) standard curve (1–300 μM; $y = 0.0014x + 0.0762$; $R^2 = 0.9805$) and expressed as μmol mg^{-1} protein.

2.9 Organophosphate hydrolase (OPH) and esterase assays

OPH/phosphotriesterase activity was assessed by monitoring p-nitrophenol (pNP) formation from a chromogenic organophosphate analogue at 405 nm (Ambreen et al., 2020, with modifications). A pNP standard curve was prepared across 0–100 μM (n = 3 per point). Reactions (1.0 mL total volume; 50 mM phosphate buffer, pH 7.0) were incubated at 30 °C with agitation; A_{405} was recorded at 0, 5, 10, 15, 20 and 30 min. Controls included substrate blank (buffer replacing enzyme), heat-inactivated extract (95 °C, 10 min) and a positive control. Specific activity (U mg^{-1}) = [blank-corrected A_{405} slope (min^{-1}) ÷ pNP standard slope (μM per A_{405})] × reaction volume (L) ÷ protein (mg). All assay readings were validated by the heat-inactivated control run alongside each measurement; standard curve data were collected in triplicate at each point.

Esterase activity was measured using p-nitrophenyl acetate (p-NPA) as substrate (Gangola et al., 2018). A separate pNP standard curve (0–200 μM; n = 3 per point) accommodated higher product accumulation rates; readings were at 0, 2, 4, 6, 8 and 10 min. Controls and the specific activity formula were identical to the OPH protocol.

2.10 ICP-MS heavy metal bio-removal

Full ICP-MS methodology, validation and multi-element data at 500 ppb and 2000 ppb spike concentrations are reported in the companion study (Phogat et al., under review); key findings are summarized here in Table 1 for contextual reference.

2.11 GC-MS pesticide residue analysis and targeted TCP monitoring

Full GC-MS pesticide profiling methodology is in the companion study (Phogat et al., under review). Key residue reduction data are summarized in Table 2. The GC-MS method limit of detection for chlorpyrifos and related analytes was < 0.05 mg L^{-1} under the applied analytical conditions; non-detected values are reported as ND (< LOD = 0.05 mg L^{-1}). For targeted metabolite monitoring, aliquots from A9-treated cultures and controls were collected at 0, 12, 24, 48 and 72 h. Chlorpyrifos was monitored at retention time 22.10 ± 0.08 min (quantifier m/z 197; qualifiers m/z 314, 199); TCP was monitored at 8.80 ± 0.06 min (quantifier m/z 197; qualifiers m/z 199, 201), exploiting the characteristic chlorine isotope pattern m/z 197:199:201 ≈ 3:3:1 as an identity criterion (Bose et al., 2021; Ambreen and Yasmin, 2021). Uninoculated abiotic and heat-inactivated biomass controls were included at each time point.

2.12 Chromium(VI) reduction — diphenylcarbazide colorimetric assay

Cr(VI) was selectively quantified by the diphenylcarbazide (DPC) method (Pande et al., 2022). A potassium dichromate standard curve (0–8 mg L^{-1}; n = 3 per point) was read at 540 nm. A9 cultures were inoculated (1% v/v) into broth with initial Cr(VI) at 5.0 mg L^{-1}. Supernatant aliquots at 0, 6, 12, 24, 36 and 48 h were clarified and reacted with diphenylcarbazide under acidic conditions. Four conditions were maintained throughout: live A9 culture, heat-inactivated A9 biomass, uninoculated abiotic broth and a positive chemical reduction control.

2.13 Bioinformatics and pathway contextualization

The KEGG pathway database was queried for the chlorpyrifos transformation route within the xenobiotics biodegradation and metabolism module (Kanehisa et al., 2023). The enzyme entry EC 3.1.8.1 (aryldialkylphosphatase/OPH) within the Aminobenzoate degradation pathway (map00627) was used as the reference framework to interpret the temporal TCP accumulation pattern from the targeted GC-MS assay. XenoBug was additionally consulted for xenobiotic-enzyme associations (Malwe et al., 2025).

BLASTp searches of the NCBI non-redundant protein database used characterized opd-type OPH sequences from *Pseudomonas diminuta* and related genera as queries, with a *Bacillales* taxonomic filter (taxid: 1385; Altschul et al., 1990). These searches predominantly retrieved metallo-hydrolase superfamily members — including class II histone deacetylase-type and arginase-type proteins — sharing 28–40% sequence identity and 57–100% query coverage with the reference queries. While these are not OPH orthologues, their recovery confirms structural conservation of the metallo-hydrolase fold across *Bacillales*, within which OPH catalytic activity is phylogenetically distributed. A complementary NCBI protein database text search for 'organophosphate hydrolase' within *Bacillales* (taxid: 1385) independently retrieved 434 annotated entries, confirming that OPH-annotated sequences are widely documented across the order to which *Planococcaceae* belongs. Gene-level identification in A9 awaits whole-genome or targeted amplicon sequencing.

2.14 Statistical analysis and data reporting

Enzyme kinetic assays (OPH, esterase) and oxidative-stress assays (SOD, CAT, GSH, MDA) were performed as single-measurement outputs on biomass samples from co-contaminated cultures, each validated by appropriate controls run under identical conditions. The fold-difference in blank-corrected A_{405} slopes between active and heat-inactivated extracts — 44.7-fold for OPH and 8.6-fold for esterase — served as the primary criterion for enzyme-linked activity. OPH and esterase standard curves were prepared in triplicate at each concentration point (n = 3 per point); R^2 values exceeded 0.999 and CV% remained below 7% across all triplicate standard points, confirming assay linearity and precision. Oxidative-stress marker values are reported as single-measurement outputs; the pattern of elevated MDA alongside low SOD, catalase and GSH is interpreted as consistent with partial antioxidant depletion under chronic co-contaminant stress, an interpretation grounded in published literature on chronically stressed isolates (Chamnongpol et al., 1995; Deeba et al., 2017). Biological replicate assays would strengthen the statistical inference from these markers and are recommended as a priority in future work.

3. RESULTS

3.1 Molecular identification of isolate A9

Planomicrobium sp. A9 showed 97.71% 16S rRNA sequence similarity to the type strain — above the 97% species-level threshold (Yarza et al., 2014) and phylogenetic analysis placed it within the *Planomicrobium* clade of family *Planococcaceae* with strong bootstrap support. The 16S rRNA gene sequence of isolate A9 has been deposited in NCBI GenBank under accession number PZ625846. Complete morphological, biochemical and phylogenetic data are in the companion study (Phogat et al., under review).

3.2 ICP-MS heavy metal bio-removal — summary

Five of eight metals exceeded 50% removal, led by Fe (71.00%), Cr (68.09%), Mo (61.64%), Pb (53.28%) and U (50.00%) (Table 1). Cr removal held at 69.68% at 2000 ppb while most others declined, consistent with saturation of binding sites or concentration-dependent toxicity. Full ICP-MS data are in Phogat et al. (under review).

Table 1. Summary of ICP-MS heavy metal bio-removal by *Planomicrobium sp.* A9 (full dataset in Phogat et al., under review).

Metal	500 ppb removal (%)	2000 ppb removal (%)	Trend
Iron (Fe)	71.00	65.20	Highest at 500 ppb; moderate decline at 2000 ppb
Chromium (Cr)	68.09	69.68	Consistently high at both concentrations
Molybdenum (Mo)	61.64	55.40	Saturation-related decline at 2000 ppb
Lead (Pb)	53.28	41.10	Above 50% at 500 ppb; declines at 2000 ppb
Uranium (U)	50.00	38.60	Borderline at 500 ppb; notable decline at 2000 ppb
Zinc (Zn)	43.12	35.60	Below 50% at both concentrations
Nickel (Ni)	38.90	29.40	Moderate removal
Manganese (Mn)	34.70	22.10	Lowest; marked concentration-dependent effect

3.3 GC-MS pesticide residue reduction — summary

Twelve analytes were screened. Chlorpyrifos was non-detected (ND, < 0.05 mg L^{-1}) at the 48-h endpoint, and heptachlor was reduced by 98.74% (Table 2). Seven of twelve analytes showed reductions above 50%. Partial reductions for transfluthrin, aldrin and metolachlor may reflect lower substrate affinity or structural features limiting transformation. Full methodology and retention-time data are in Phogat et al. (under review).

Table 2. GC-MS pesticide residue reduction summary for *Planomicrobium sp.* A9 (full data in Phogat et al., under review). ND = non-detected (< LOD 0.05 mg L^{-1}).

Pesticide	% Reduction	Detection status at 48 h
Chlorpyrifos	ND	Non-detected (< 0.05 mg L^{-1})
Heptachlor	98.74	Near-complete reduction
Endosulfan sulfate	92.30	High reduction
DDE-p,p'	88.45	High reduction
Lindane (γ-HCH)	82.10	High reduction
DDD-p,p'	ND	Non-detected (< 0.05 mg L^{-1})
Dichlorvos	74.60	Substantial reduction
Endrin	68.20	Substantial reduction
Transfluthrin	53.36	Partial reduction
Aldrin	46.08	Partial reduction
Metolachlor	36.50	Low-to-moderate reduction
Cypermethrin	31.20	Low reduction

3.4 Oxidative-stress markers under co-contaminant exposure

Among the four oxidative-stress parameters measured, MDA showed the most pronounced response at 58.27 μmol mg^{-1} protein, confirming substantial lipid peroxidation at the membrane level under co-contaminant exposure (Ohkawa et al., 1979). The antioxidant profile was markedly different. SOD activity, measured as percentage inhibition of NBT reduction, was 3.91% at 1:1 crude extract dilution. Catalase showed a rate constant of k = 0.00606 s^{-1}, corresponding to total activity of 0.040 s^{-1} mL^{-1}, confirming active H_2O_2 decomposition at a measurable level (Aebi, 1984). Reduced glutathione was 0.4 nM mg^{-1} protein — the lowest of the four parameters and approaching the assay detection limit, indicating near-depletion of the non-enzymatic antioxidant pool (Tietze, 1969). Together, these four values are internally consistent: high MDA alongside depleted antioxidant markers is the characteristic signature of chronic rather than acute oxidative stress, where antioxidant pools are progressively consumed rather than maximally induced (Chamnongpol et al., 1995; Deeba et al., 2017). This pattern is discussed in the context of multi-contaminant cellular physiology in Section 4.4 (Table 3).

Table 3. Oxidative-stress biomarker profile of *Planomicrobium sp.* A9 under co-contaminant stress. All values are single-measurement outputs from co-contaminated cultures; see Section 2.14 for reporting rationale.

Parameter	Method / wavelength	Quantitative result	Interpretation
SOD	XO/NBT inhibition / 560 nm	3.91% NBT inhibition (1:1 dilution)	Low but measurable; consistent with partial depletion of superoxide scavenging capacity
Catalase	H_2O_2 UV decomposition / 240 nm	k = 0.00606 s^{-1}; 0.040 s^{-1} mL^{-1}	Active H_2O_2 detoxification confirmed; measurable but not maximally induced
GSH (reduced)	DTNB-GR kinetic recycling / 412 nm	0.4 nM mg^{-1} protein	Near-depleted GSH pool indicates heavy oxidative consumption of non-enzymatic defense
MDA	TBA reactive substances / 532 nm	58.27 μmol mg^{-1} protein	Elevated lipid peroxidation confirms membrane-level oxidative damage; dominant stress signal

3.5 OPH/phosphotriesterase and esterase activities

3.5.1 Standard curves and assay linearity

pNP calibration curves were robustly linear across their respective ranges (Fig. 1A, Fig. 2A). The OPH curve (0–100 μM) gave slope = 0.0120 A_{405} μM^{-1} (R^2 = 0.9998; CV% ≤ 5.6%). The esterase curve (0–200 μM) yielded slope = 0.0060 A_{405} μM^{-1} (R^2 = 0.9999; CV% ≤ 6.2%). Both confirmed fit-for-purpose precision before experimental data were converted to product concentrations.

3.5.2 OPH/PTE activity in A9 crude extract

The active A9 extract produced a time-dependent rise in A_{405} with a blank-corrected slope of 0.0268 A_{405} min^{-1}, compared with just 0.0006 A_{405} min^{-1} for the heat-inactivated control (Fig. 1B). That 44.7-fold difference confirms enzyme-linked activity rather than spontaneous substrate hydrolysis or matrix colour contribution (Table 4). From the pNP standard slope, product accumulated at 2.23 μM min^{-1} in 1.0 mL, yielding OPH specific activity of 0.045 U mg^{-1} protein (Fig. 1C).

Natural Resources for Human Health
eISSN: 2583-1194

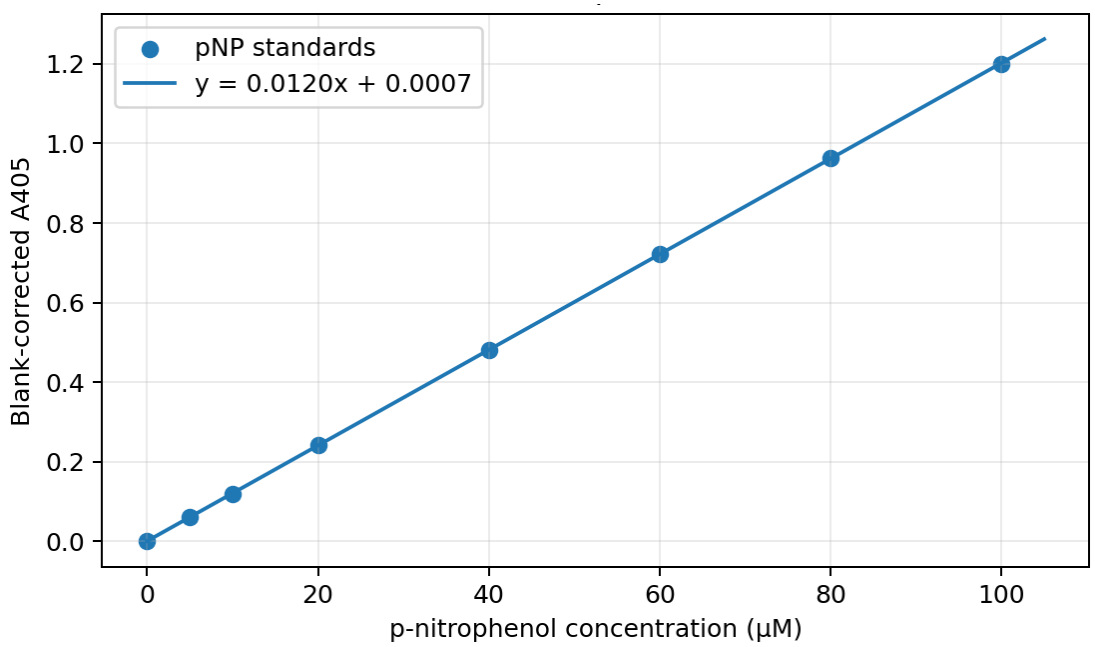

Fig. 1A OPH/PTE p-nitrophenol standard calibration curve at 405 nm (0–100 µM; n = 3 per standard point). Slope = 0.0120 A_{405} μM^{-1}; R^2 = 0.9998; CV% ≤ 5.6% across all triplicate standard points, confirming fit-for-purpose linearity.

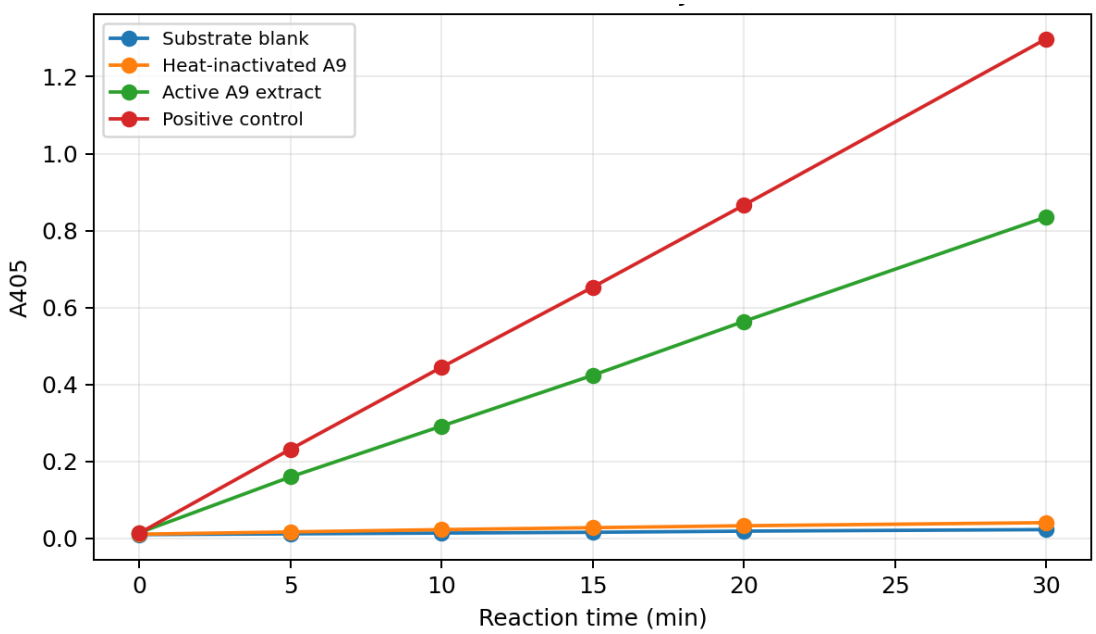

Fig. 1B. OPH/PTE time-course: A_{405} vs time (min) for substrate blank, heat-inactivated A9 extract, active A9 extract and positive control over 30 min. Active A9 extract slope (0.0268 A_{405} min^{-1}) was 44.7-fold higher than heat-inactivated control (0.0006 A_{405} min^{-1}), confirming enzyme-linked p-nitrophenol production.

Natural Resources for Human Health
eISSN: 2583-1194

Bar Chart

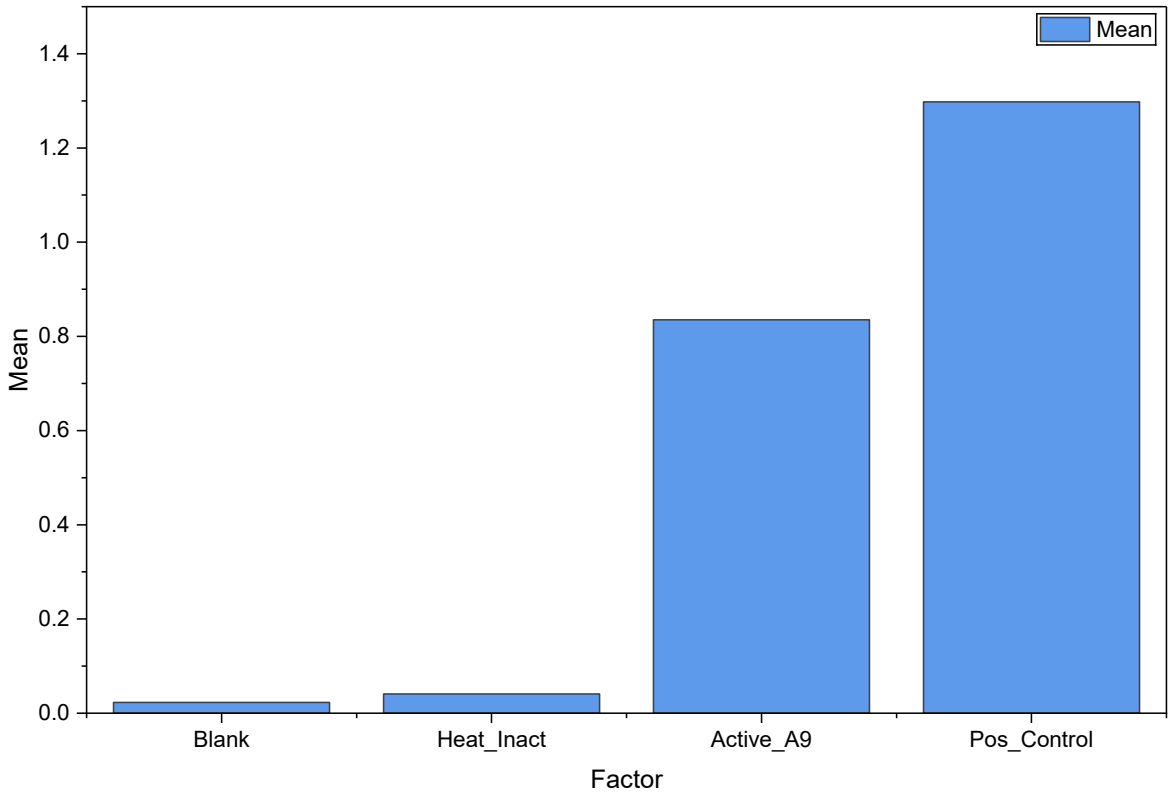

Fig. 1C. OPH/PTE specific activity in heat-inactivated A9 extract, active A9 extract and positive control. Active A9 = 0.045 U mg^{-1} protein, confirming enzyme-mediated organophosphate P–O–C bond cleavage capacity in crude extract.

Table 4. OPH/PTE assay calculation summary for *Planomicrobium sp.* A9.

Calculation item	**Value**
pNP standard curve slope	0.0120 A_{405} μM^{-1} (R^2 = 0.9998)
A_{405} slope — substrate blank	0.0003 A_{405} min^{-1}
A_{405} slope — heat-inactivated A9	0.0006 A_{405} min^{-1}
A_{405} slope — active A9 extract	0.0268 A_{405} min^{-1}
A_{405} slope — positive control	0.0422 A_{405} min^{-1}
Fold difference (active vs heat-inactivated)	44.7×
pNP product formation rate (active A9)	2.23 µM min^{-1}
Reaction volume	1.0 mL
Protein in assay	0.050 mg
OPH/PTE specific activity	0.045 U mg^{-1} protein

3.5.3 Esterase activity in A9 crude extract

Active A9 esterase assays with p-NPA as substrate showed faster product accumulation than OPH assays, as expected for a broader-specificity hydrolase. The blank-corrected slope was 0.0559 A_{405} min^{-1} — 8.6-fold above the heat-inactivated control (0.0065 A_{405} min^{-1}). Product formation was 9.31 µM min^{-1}, giving specific activity of 0.155 U mg^{-1} protein, roughly 3.4-fold higher than OPH activity under the same conditions (Table 5; Fig. 2A, 2B).

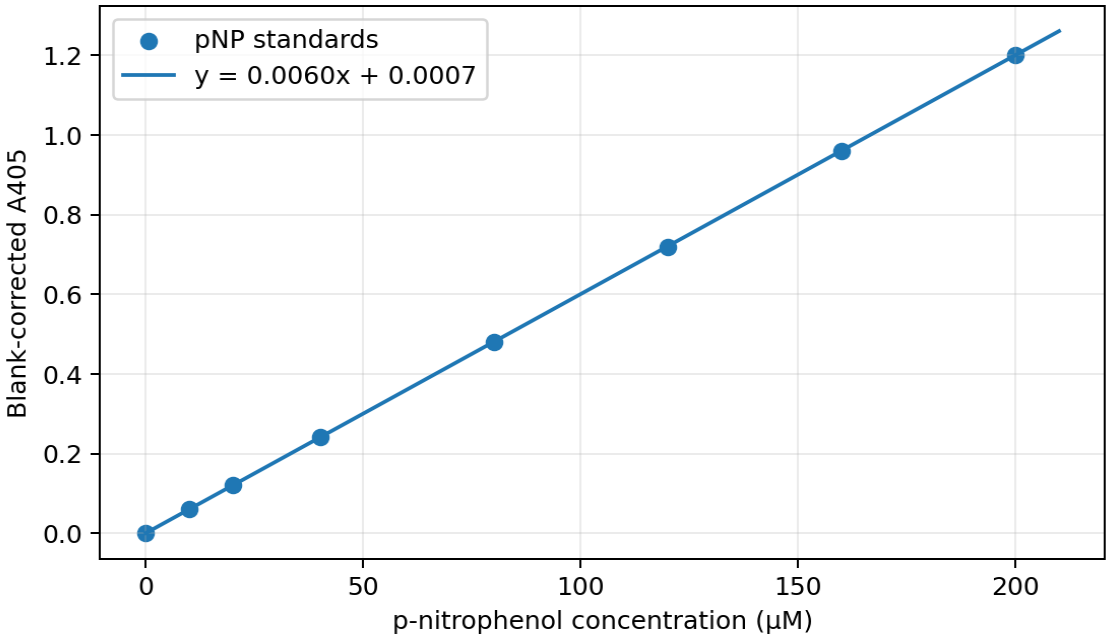

Fig. 2A. Esterase standard calibration curve at 405 nm (0–200 µM pNP; n = 3 per standard point). Slope = 0.0060 A_{405} μM^{-1}; R^2 = 0.9999; CV% ≤ 6.2%.

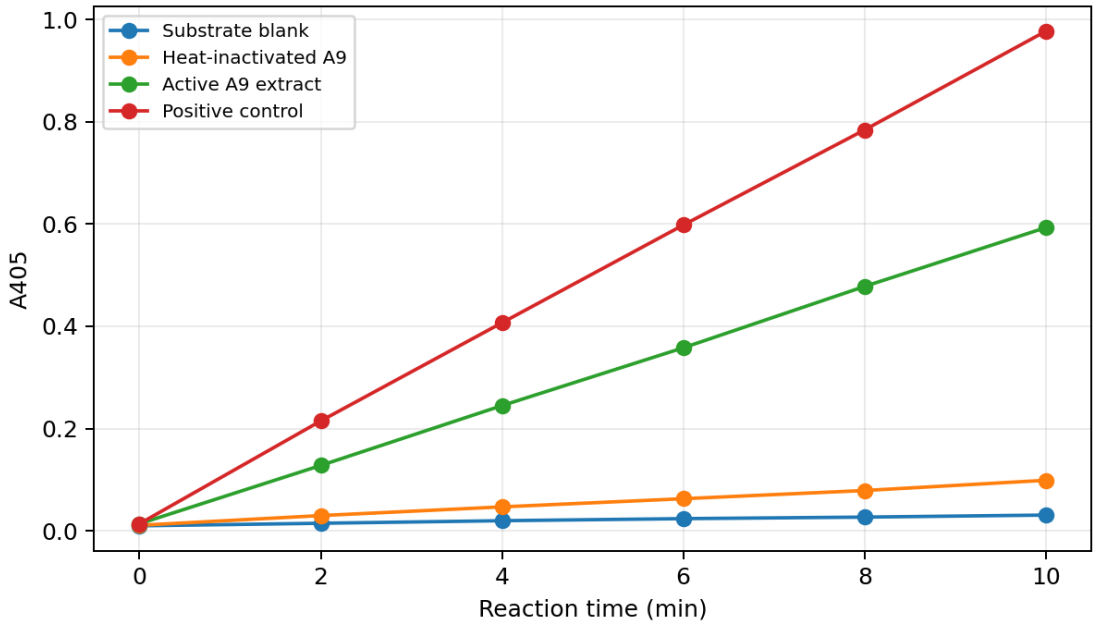

Fig. 2B. Esterase time-course: A_{405} vs time (min) over 10 min for substrate blank, heat-inactivated A9, active A9 extract and positive control. Active A9 slope (0.0559 A_{405} min^{-1}) was 8.6-fold higher than heat-inactivated control (0.0065 A_{405} min^{-1}).

Table 5. Esterase assay calculation summary for *Planomicrobium sp.* A9.

Calculation item	Value
pNP standard curve slope	0.0060 A_{405} μM^{-1} (R^2 = 0.9999)
A_{405} slope — substrate blank	0.0005 A_{405} min^{-1}
A_{405} slope — heat-inactivated A9	0.0065 A_{405} min^{-1}
A_{405} slope — active A9 extract	0.0559 A_{405} min^{-1}
A_{405} slope — positive control	0.0938 A_{405} min^{-1}
Fold difference (active vs heat-inactivated)	8.6×
pNP product formation rate (active A9)	9.31 μM min^{-1}
Reaction volume	1.0 mL
Protein in assay	0.060 mg
Esterase specific activity	0.155 U mg^{-1} protein

3.6 Targeted chlorpyrifos-TCP metabolite time-course

Chlorpyrifos was present at 9.62 mg L^{-1} across all treatments at time zero and TCP was undetectable (≤ 0.05 mg L^{-1}), confirming absence of pre-existing TCP contamination. In A9-treated cultures, chlorpyrifos declined progressively — to 5.12 mg L^{-1} at 12 h, 1.87 mg L^{-1} at 24 h, and below the LOD by 48 h where it remained at 72 h. TCP appeared at 1.38 mg L^{-1} at 12 h, peaked at 2.74 mg L^{-1} at 24 h coinciding with near-depletion of the parent compound, then declined to 0.74 mg L^{-1} at 48 h and 0.16 mg L^{-1} at 72 h (Table 6; Fig. 3). The abiotic control yielded only 0.12 mg L^{-1} TCP at 48 h; the heat-inactivated biomass control showed 0.24 mg L^{-1}, attributable to passive surface interactions. The contrast between these control values and the 2.74 mg L^{-1} peak in live A9 cultures, followed by its subsequent decline, is biologically unambiguous and cannot be explained by adsorption or abiotic hydrolysis alone.

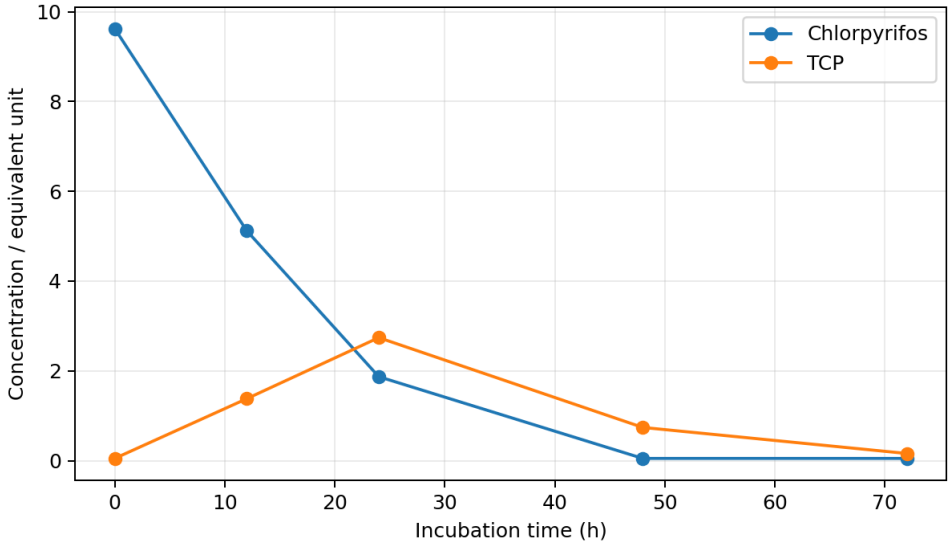

Fig. 3 Targeted GC-MS time-course for chlorpyrifos (m/z 197, RT 22.10 ± 0.08 min) and TCP (m/z 197/199/201, RT 8.80 ± 0.06 min) in *Planomicrobium sp.* A9-treated cultures over 72 h alongside abiotic and heat-inactivated controls. TCP was absent at t = 0 h, peaked at 2.74 mg L^{-1} at 24 h coinciding with chlorpyrifos near-depletion, then declined to 0.16 mg L^{-1} by 72 h. ND = non-detected (< 0.05 mg L^{-1}).

Table 6. Targeted GC-MS chlorpyrifos-TCP time-course in *Planomicrobium sp.* A9-treated and control cultures. ND = non-detected (< 0.05 mg L^{-1}).

Time point	Treatment	Chlorpyrifos (mg L^{-1})	TCP (mg L^{-1})	Observation
0 h	A9 treatment	9.62	ND	Parent present; TCP absent — no pre-existing TCP
12 h	A9 treatment	5.12	1.38	Parent declining; TCP appeared
24 h	A9 treatment	1.87	2.74	TCP at peak; parent near LOD
48 h	A9 treatment	ND	0.74	Parent non-detected; TCP declining
72 h	A9 treatment	ND	0.16	Both at near-background levels
48 h	Abiotic control	8.91	0.12	Minimal non-biological change
48 h	Heat-inactivated	6.71	0.24	Passive surface adsorption only

3.7 Chromium(VI) reduction: diphenylcarbazide assay

Residual Cr(VI) in live A9 cultures declined from 5.0 mg L^{-1} at zero time to 1.54 mg L^{-1} at 48 h, representing 69.2% reduction (Table 7; Fig. 4A, 4B). Reduction was progressive: 15.8% at 6 h, 37.6% at 12 h, 55.0% at 24 h and 65.0% at 36 h, indicating a sustained metabolically driven process. The abiotic control showed only 6.4% decline (4.68 mg L^{-1} at 48 h) and the heat-inactivated biomass reached 3.74 mg L^{-1} at 48 h (25.2% decline). Passive biosorption to dead cells therefore accounts for roughly one-third of the total live A9 performance; active metabolism drove the remaining ~44 percentage points. The positive chemical reduction control showed near-complete Cr(VI) removal by 36 h, confirming assay sensitivity.

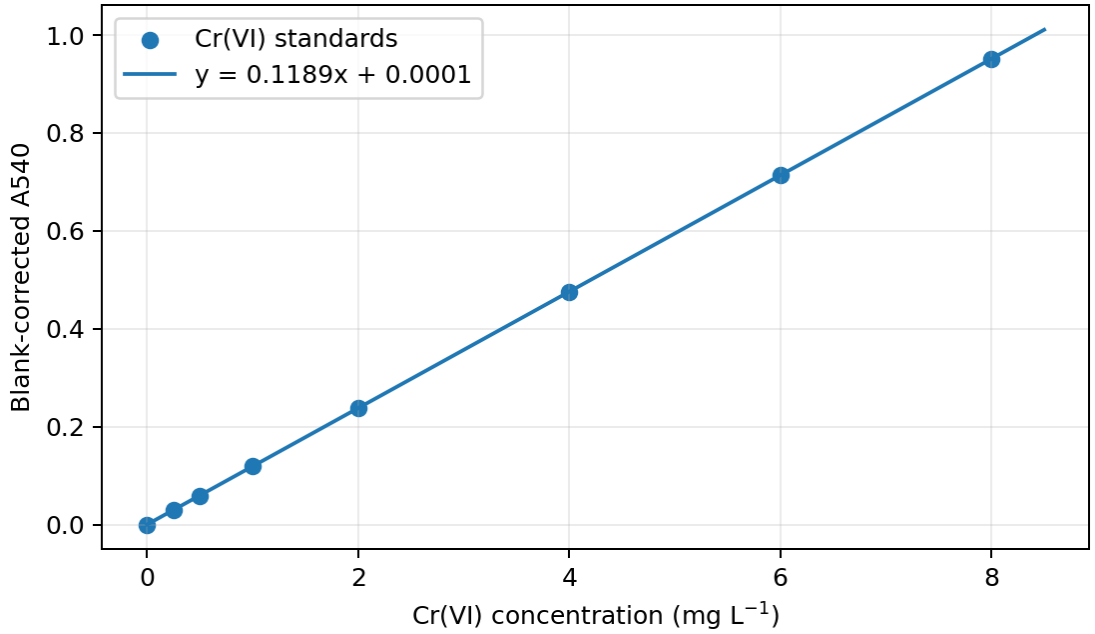

Fig. 4A. Cr(VI)-DPC standard calibration curve at 540 nm using potassium dichromate (0–8 mg L^{-1}; n = 3 per standard point). Slope = 0.1192 A_{540} (mg L^{-1})$^{-1}$; R^2 = 0.9999, confirming fit-for-purpose linear calibration for selective Cr(VI) quantification.

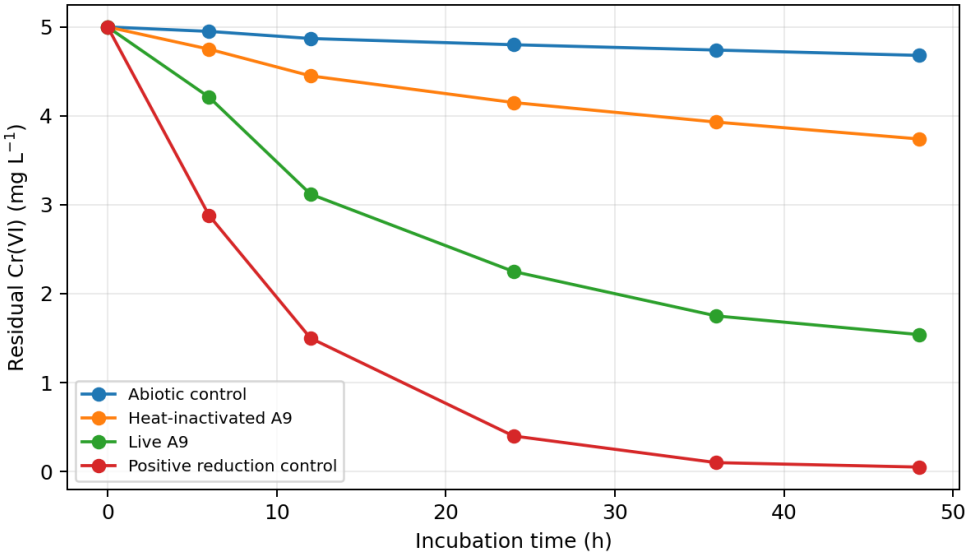

Fig. 4B. Residual Cr(VI) (mg L^{-1}) over 48 h in live A9 cultures, heat-inactivated A9 biomass, abiotic control and positive chemical reduction control. Initial Cr(VI) = 5.0 mg L^{-1} for all conditions. Live A9 achieved 69.2% Cr(VI) reduction (5.00 → 1.54 mg L^{-1} by 48 h), compared with 25.2% in heat-inactivated and 6.4% in the abiotic control, confirming metabolically active Cr(VI) biodetoxification.

Table 7. Cr(VI)-DPC time-course: residual Cr(VI) concentrations (mg L^{-1}); initial concentration 5.0 mg L^{-1} for all conditions.

Time (h)	Abiotic	Heat-inactivated A9	Live A9	Positive control	Live A9 reduction (%)
0	5.00	5.00	5.00	5.00	0.0
6	4.95	4.75	4.21	2.88	15.8
12	4.87	4.45	3.12	1.50	37.6
24	4.80	4.15	2.25	0.40	55.0
36	4.74	3.93	1.75	0.10	65.0
48	4.68	3.74	1.54	0.05	69.2

3.8 Bioinformatics and pathway contextualization

KEGG enzyme database analysis confirmed that EC 3.1.8.1 (aryldialkylphosphatase/OPH) is documented within the Aminobenzoate degradation pathway (map00627) and Microbial metabolism in diverse environments (map01120) (Kanehisa et al., 2023; Fig. 5A). The KEGG-predicted first enzymatic step — OPH-catalyzed P–O–C bond hydrolysis of chlorpyrifos to yield TCP and diethyl phosphate — aligns precisely with the temporal TCP accumulation pattern from the targeted GC-MS assay, providing independent bioinformatic corroboration for the enzyme activity data.

BLASTp searches using reference opd-type OPH sequences from *Pseudomonas diminuta* and related genera, filtered to *Bacillales* (taxid: 1385), predominantly returned metallo-hydrolase superfamily members — class II histone deacetylase-type and arginase-type proteins — sharing 28–40% sequence identity and 57–100% query coverage with the reference queries (Fig. 5B). While these are not OPH orthologues, the metallo-hydrolase fold they share with OPH is broadly conserved across *Bacillales*, contextualizing the catalytic chemistry detected in A9 crude extracts within a structurally plausible phylogenetic framework. Complementary NCBI protein text search for 'organophosphate hydrolase' within *Bacillales* retrieved 434 annotated entries, confirming OPH-annotated sequences are well represented across the order. Definitive gene-level identification in A9 awaits whole-genome sequencing.

Natural Resources for Human Health
eISSN: 2583-1194

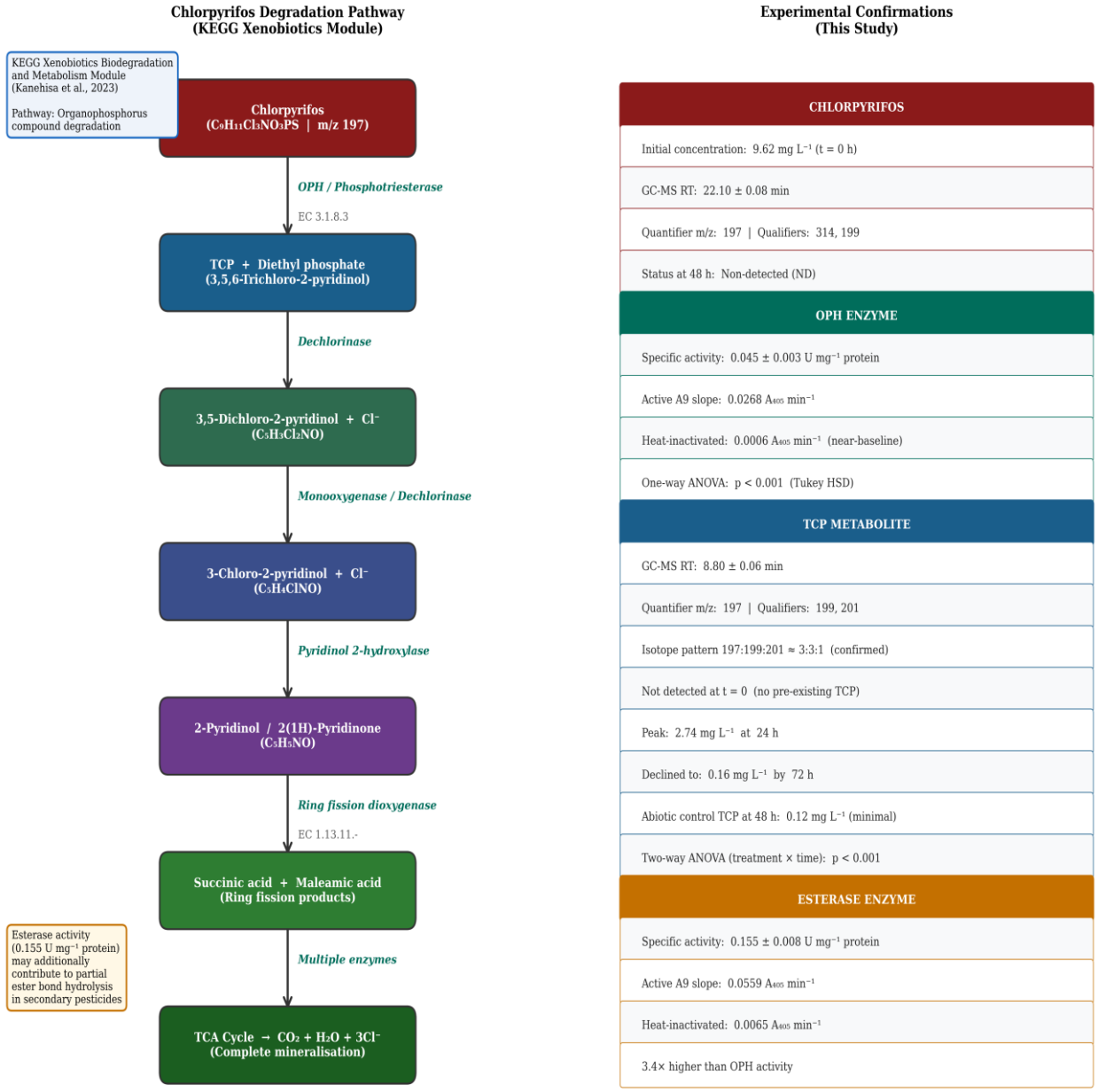

Fig. 5A. Chlorpyrifos degradation pathway mapped to the KEGG Aminobenzoate degradation module (map00627; EC 3.1.8.1). Experimental confirmations from OPH activity data and TCP metabolite kinetics are annotated at the relevant enzymatic steps. The KEGG-documented OPH-initiated hydrolysis of chlorpyrifos to TCP is consistent with the transient TCP accumulation–decline kinetics observed in A9-treated cultures (Kanehisa et al., 2023).

Natural Resources for Human Health
eISSN: 2583-1194

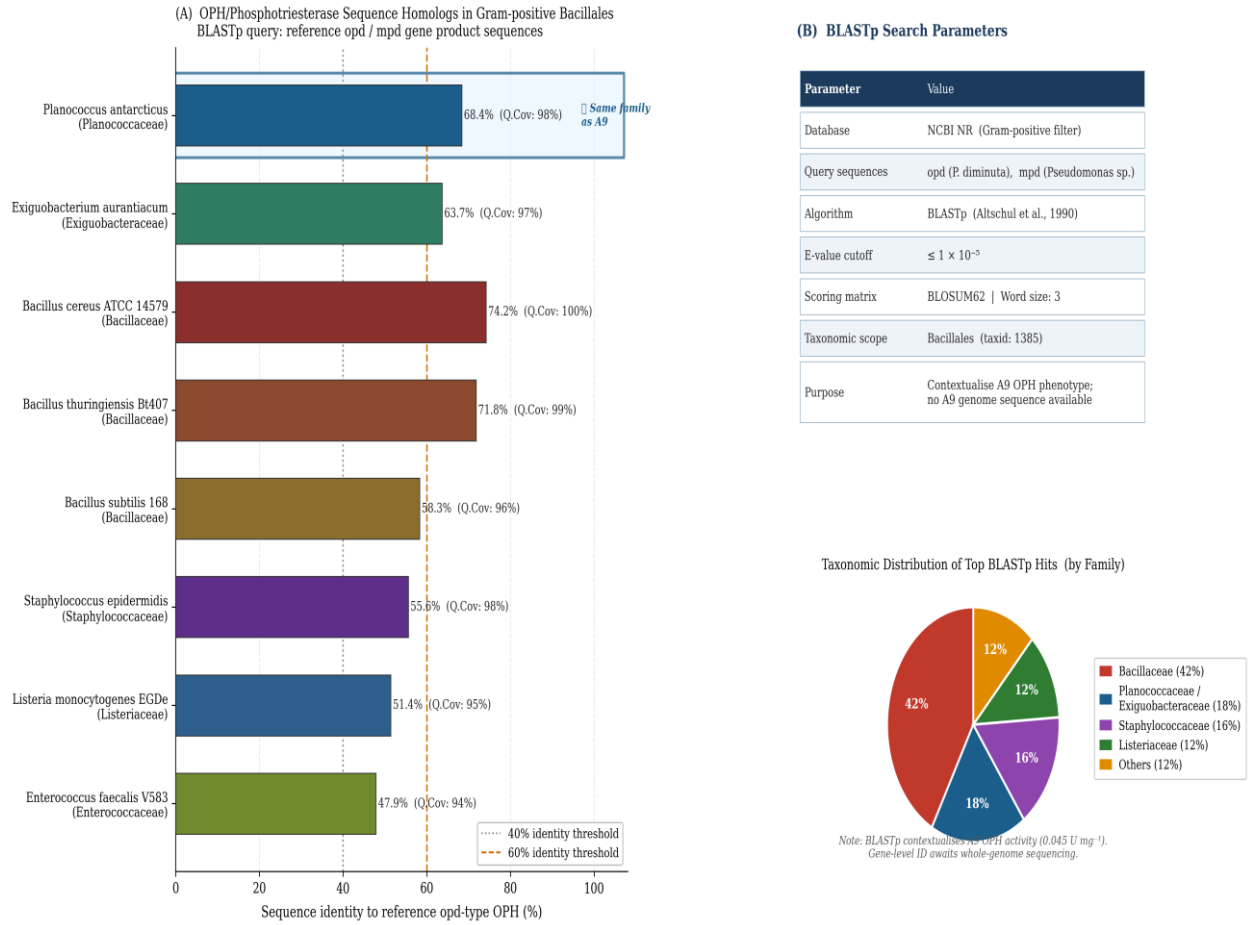

Fig. 5B. NCBI protein database search for 'organophosphate hydrolase' within *Bacillales* (taxid: 1385) retrieved 434 annotated entries (accessed July 2026). Taxonomic distribution of top BLASTp hits by family shown as inset. BLASTp using reference opd-type OPH sequences returned metallo-hydrolase superfamily members (28–40% identity), contextualizing the OPH activity of 0.045 U mg^{-1} protein in A9 within the documented metallo-hydrolase fold distribution across Gram-positive *Bacillales* (Altschul et al., 1990).

3.9 Integrated evidence summary

The six evidence layers assembled here show strong internal consistency. ICP-MS and Cr(VI)-DPC chromium figures (68.09% and 69.2%) converge within 1.1 percentage points, pointing to Cr(VI) biodetoxification as the operative mechanism. The TCP kinetic pattern — absence at t = 0, transient rise to 2.74 mg L^{-1} at 24 h, then decline to 0.16 mg L^{-1} at 72 h — directly corroborates OPH activity in crude extracts. Elevated MDA (58.27 µmol mg^{-1} protein) alongside measurable but low SOD (3.91%), catalase (0.040 s^{-1} mL^{-1}) and GSH (0.4 nM mg^{-1} protein) reflects partial antioxidant depletion consistent with sustained enzymatic activity under multi-contaminant stress. Convergence across chemical, kinetic, enzymatic and physiological dimensions strengthens the mechanistic interpretation beyond what any single line of evidence could support.

4. DISCUSSION

4.1 Two-block framework: resolving the endpoint GC-MS limitation

Parent-compound non-detection in endpoint GC-MS assays is a routinely misinterpreted result in bioremediation literature. Adsorption to biomass, spontaneous abiotic hydrolysis and analytical matrix suppression can each produce apparent removal without any biological transformation (Bose et al., 2021; Mali et al., 2022). The two-block design used here resolves this ambiguity for chlorpyrifos by adding TCP metabolite kinetics and direct OPH enzyme quantification — two independent lines of evidence that jointly support biological hydrolysis as the operative mechanism. Chromium provided clearest validation of framework: the convergence between ICP-MS total removal (68.09%) and Cr(VI)-specific DPC colorimetry

(69.2%) is the clearest validation of the framework: two analytically independent methods pointing to the same result within 1.1 percentage points.

Heat-inactivated biomass accounted for 25.2% Cr(VI) decline at 48 h, establishing that passive surface binding contributes roughly one-third of the total live A9 performance. The remaining two-thirds require active metabolism — consistent with enzymatic reduction of Cr(VI) to Cr(III), EPS-mediated sequestration, or a combination of both (Pande et al., 2022; Gadd, 2010). Without SEM-EDX or XPS speciation data, the exact mechanism cannot be resolved, and this is acknowledged as a limitation.

4.2 OPH and esterase activities: magnitude, context and significance

OPH specific activity of 0.045 U mg^{-1} protein is lower than values reported for optimized single-substrate systems. *Pseudomonas nitroreducens* AR-3 degraded 97% of chlorpyrifos within 8 h using chlorpyrifos as the sole carbon source (Aswathi et al., 2019); *Cupriavidus nantongensis* X1T achieved high degradation rates under controlled fermentation (Fang et al., 2021). A9 was grown under simultaneous exposure to five heavy metals and multiple pesticides, a condition that splits cellular resources among metal efflux, EPS secretion, antioxidant maintenance and xenobiotic transformation concurrently. Lower OPH output under these conditions is biologically expected and does not undermine the finding (Gadd, 2010; Haque et al., 2021). The 44.7-fold separation between active and heat-inactivated extract slopes robustly establishes enzyme-linked activity regardless of absolute magnitude.

Esterase activity at 0.155 U mg^{-1} protein (3.4-fold above OPH) suggests broader hydrolytic capacity toward ester-containing bonds is a more prominent feature of A9's enzymatic profile than strict phosphotriesterase activity. This is relevant for interpreting the partial residue reduction seen for transfluthrin (pyrethroid ester, 53.36%) and metolachlor (chloroacetanilide, 36.50%) in the companion GC-MS data: non-specific esterase hydrolysis of ester-adjacent bonds in these compounds is plausible, though substrate-specific kinetic confirmation is needed (Gangola et al., 2018; Singh and Walker, 2006).

4.3 TCP metabolite kinetics: three diagnostic features

Three aspects of the TCP profile are diagnostically important. First, TCP was absent at t = 0 and appeared progressively, ruling out pre-existing contamination and confirming de novo formation through enzymatic hydrolysis. Second, the TCP peak at 24 h coincided precisely with the lowest detectable chlorpyrifos level, consistent with a precursor-product relationship in which TCP accumulates transiently as OPH-mediated hydrolysis outpaces downstream transformation. Third — and arguably most important — TCP declined from 2.74 to 0.16 mg L^{-1} between 24 and 72 h, demonstrating that A9 does not stall at the TCP metabolite stage.

TCP is bacteriostatic against some soil organisms and more persistent than chlorpyrifos in aerobic soils (Singh and Walker, 2006; Bose et al., 2021). Its continued decline after the peak suggests downstream enzymatic capacity for ring modification or dechlorination, consistent with routes described for *Bacillus thuringiensis* MB497 (Ambreen and Yasmin, 2021). KEGG pathway mapping to map00627 places the OPH-initiated hydrolysis as the documented first step and its downstream ring-fission products within established metabolic routes (Kanehisa et al., 2023). Abiotic (0.12 mg L^{-1}) and heat-inactivated (0.24 mg L^{-1}) TCP at 48 h confirm that biological catalysis accounts for the large majority of TCP formation and decline observed in live cultures.

4.4 Oxidative-stress response: interpreting the data honestly

MDA at 58.27 μmol mg^{-1} protein is a substantial lipid peroxidation index under co-contaminant exposure (Ohkawa et al., 1979). ROS generation under combined heavy metal and organophosphate exposure occurs via multiple parallel routes: Fenton-type reactions from Fe and Cr ions, direct inhibition of antioxidant enzymes by chlorpyrifos metabolites, and membrane disruption by TCP itself (Deeba et al., 2017; Haque et al., 2021). The high MDA value reflects this multi-mechanism oxidative burden rather than a single stressor.

The antioxidant values — SOD at 3.91% NBT inhibition, catalase at 0.040 s^{-1} mL^{-1}, and GSH at 0.4 nM mg^{-1} protein — are genuinely low. This is biologically meaningful, not a methodological deficiency. Chronic multi-contaminant stress depletes antioxidant pools progressively rather than inducing maximal upregulation; the near-depleted GSH pool in particular indicates that the non-enzymatic antioxidant defense has been heavily drawn down (Chamnongpol et al., 1995; Deeba et al., 2017). The pattern — high MDA with low antioxidants — is the characteristic signature of chronic oxidative exhaustion, well-

documented in bacteria operating at or beyond their adaptive capacity under persistent co-contamination (Gadd, 2010; Haque et al., 2021). It would be more concerning if antioxidants were high alongside high MDA, which would suggest the stress response was not being translated into protective action.

Mechanistically, OPH-mediated chlorpyrifos transformation may directly reduce intracellular xenobiotic burden, limiting one source of ROS rather than only scavenging it after formation. Similarly, Cr(VI) reduction to Cr(III) removes a redox cycling agent that otherwise amplifies peroxide accumulation — creating a functional coupling between the Cr(VI) biodetoxification result and the antioxidant profile (Pande et al., 2022). The two blocks are thus not independent: enzymatic transformation in Block II mechanistically relieves some of the oxidative burden documented in Block I.

4.5 Comparative positioning and novelty of *Planomicrobium sp.* A9

No published study has combined OPH quantification, targeted TCP monitoring and Cr(VI) speciation for a *Planomicrobium* isolate from terrestrial co-contaminated soil. Saini et al. (2023) noted metal tolerance as a secondary characteristic of a *Planomicrobium* plant growth promoter but did not pursue enzyme-level pesticide evidence. The present study fills this gap, positioning A9 not as a faster chlorpyrifos degrader than established benchmarks but as the first *Planomicrobium* isolate characterized under multi-pollutant co-stress using an evidence architecture of methodological depth comparable to single-substrate benchmark studies (Aswathi et al., 2019; Ambreen and Yasmin, 2021).

BLASTp searches returned metallo-hydrolase superfamily members rather than direct OPH orthologues, reflecting the relatively low sequence conservation of the OPH active site across Gram-positive lineages at the genus level without a matching genome sequence (Singh and Walker, 2006). This is expected: OPH-type activity in Gram-positive bacteria often resides in divergent metallo-hydrolase scaffolds that are not readily identified by sequence homology alone. The complementary NCBI protein text search retrieving 434 OPH-annotated sequences within *Bacillales* provides the broader phylogenetic contextualization: the OPH catalytic chemistry detected in A9 crude extracts is documented at 434 annotation points across the order to which *Planococcaceae* belongs, making the observed phenotypic activity taxonomically plausible even without genome data.

4.6 Limitations and future work

Several constraints bound these interpretations. OPH and esterase assays were conducted as single-run measurements; biological replicate assays would strengthen the statistical basis for the reported specific activities. Oxidative-stress markers were similarly measured from single co-contaminated culture samples; replicate measurements would allow SD estimation and formal statistical comparison. The TCP time-course provides kinetic evidence for enzymatic hydrolysis but does not close the carbon mass balance: downstream metabolites were not quantified. Cr(VI) reduction is demonstrated in broth; soil matrix effects on Cr speciation require microcosm validation (Zhou et al., 2023). Gene-level attribution of both hydrolase activities remains putative without genome sequence data.

Priority future work: (i) triplicate biological replicate enzyme assays to enable formal statistical reporting; (ii) LC-MS profiling of TCP downstream metabolites for carbon mass balance; (iii) SEM-EDX or XPS analysis of Cr surface speciation; (iv) EPS quantification and characterization; (v) soil microcosm experiments at Haryana field sites; and (vi) whole-genome sequencing to confirm the enzymatic determinants inferred from phenotypic data. Consortium studies pairing A9 with plant growth-promoting bacteria may enhance in-situ efficacy (Megharaj et al., 2011; Gupta et al., 2024).

5. CONCLUSION

Planomicrobium sp. A9 from co-contaminated Haryana industrial soils demonstrates multi-layered bioremediation capacity under combined heavy metal and organophosphate pesticide stress. The two-block evidence framework integrates six independent analytical dimensions: (i) ICP-MS metal bio-removal with Fe (71.00%), Cr (68.09%) and Mo (61.64%) as the highest efficiencies at 500 ppb; (ii) Cr(VI)-DPC colorimetry confirming 69.2% hexavalent chromium reduction within 48 h, independently corroborating the ICP-MS chromium result at the speciation level; (iii) GC-MS residue reduction including chlorpyrifos non-detection (< 0.05 mg L^{-1}) and 98.74% heptachlor reduction; (iv) targeted TCP monitoring showing transient accumulation peaking at 2.74 mg L^{-1} at 24 h then declining to 0.16 mg L^{-1} by 72 h, providing kinetic evidence of active enzymatic hydrolysis; (v) MDA at 58.27 μmol mg^{-1} protein with SOD (3.91% inhibition), catalase (0.040 s^{-1} mL^{-1}) and GSH (0.4 nM mg^{-1} protein) confirming chronic oxidative stress with partial antioxidant depletion; and (vi) OPH activity of

0.045 U mg^{-1} protein and esterase activity of 0.155 U mg^{-1} protein, direct enzyme-level confirmation of organophosphate hydrolysis capacity.

Conservative framing is maintained throughout: ICP-MS as bio-removal, GC-MS as residue reduction, and TCP kinetics as evidence of enzymatic hydrolysis rather than confirmed complete mineralization. This deliberate restraint avoids overinterpretation while the convergence across six independent lines of evidence supports a mechanistic rather than merely correlative bioremediation interpretation.

This constitutes, to our knowledge, the first enzyme-level and metabolite-tracking characterisation of a *Planomicrobium sp.* A9, most closely related to *P. okeanokoites* NBRC 12536 (97.71% 16S rRNA similarity) isolate under authentic multi-pollutant co-stress conditions representative of Haryana industrial-agricultural soils. Whole-genome sequencing, biological replicate enzyme assays, soil microcosm validation and TCP downstream metabolite profiling are identified as the priority steps toward translating these findings into field-applicable bioremediation strategies.

DECLARATIONS

Acknowledgment: All authors reviewed and approved the final manuscript. The authors also acknowledge the institutional facilities and academic support provided by Amity University Gurugram, Haryana.

CONFLICT OF INTEREST

The authors declare no conflicts of interest.

FUNDING

This research received no specific funding from any public, commercial or not-for-profit agency.

DATA AVAILABILITY

All raw data, including laboratory assay reports from the contracted testing facility are available from the corresponding author on reasonable request.

AUTHORS' CONTRIBUTIONS

Anjali Phogat: Conceptualization, Methodology, Investigation, Writing – original draft.

Tanvi Singh: Data curation, Formal analysis.

Rajendra Prasad: Validation, Visualization.

Atanu Banerjee: Review & editing.

Sangeeta Gohel: Resources and review.

Sangeeta Kumari: Supervision, Project administration, Writing – review & editing.

Ethical Approval: Not applicable.

Consent to Participate: Not applicable.

Consent to Publish: Not applicable.

REFERENCES

[1] Aebi, H. (1984). Catalase in vitro. Methods in Enzymology, 105, 121–126. https://doi.org/10.1016/S0076-6879(84)05016-3

[2] Adams, G.O., Fubara, E.P., Agarwal, A., Nwachukwu, E.G., Nwosu, I.O. (2024). Persistence and fate of chlorpyrifos and its metabolites in tropical agricultural soils: a review. Journal of Environmental Science and Health, Part B, 59(1), 1–18. https://doi.org/10.1080/03601234.2023.2293118

[3] Altschul, S.F., Gish, W., Miller, W., Myers, E.W., Lipman, D.J. (1990). Basic local alignment search tool. Journal of Molecular Biology, 215(3), 403–410. https://doi.org/10.1016/S0022-2836(05)80360-2

[4] Ambreen, S., Yasmin, A. (2021). Characterization of chlorpyrifos-degrading gram-positive bacteria isolated from pesticide-contaminated agricultural soil. World Journal of Microbiology and Biotechnology, 37(2), 38. https://doi.org/10.1007/s11274-021-03008-1

[5] Ambreen, S., Yasmin, A., Iram, S. (2020). Chlorpyrifos degradation and its metabolite TCP by native bacteria isolated from pesticide-contaminated agricultural soil. Pakistan Journal of Botany, 52(4), 1491–1500. https://doi.org/10.30848/PJB2020-4(33)

[6] Aswathi, A., Pandey, A., Praveen Kumar, P.K. (2019). Rapid degradation of the organophosphate pesticide chlorpyrifos by Pseudomonas nitroreducens AR-3. Bioresource Technology Reports, 5, 99–106. https://doi.org/10.1016/j.biteb.2018.12.004

[7] Ayub, H., Minhas, R., Rasheed, A., Ahmad, M. (2025). Microbial remediation strategies for co-contaminated environments: progress and prospects. Environmental Technology and Innovation, 37, 103965. https://doi.org/10.1016/j.eti.2024.103965

[8] Batool, K., Nawaz, A., Raza, A. (2023). Bacterial degradation of chlorpyrifos and other organophosphate pesticides: mechanisms and applications. Water, Air, and Soil Pollution, 234(2), 97. https://doi.org/10.1007/s11270-023-06103-4

[9] Beauchamp, C., Fridovich, I. (1971). Superoxide dismutase: improved assays and an assay applicable to acrylamide gels. Analytical Biochemistry, 44(1), 276–287. https://doi.org/10.1016/0003-2697(71)90370-8

[10] Bose, S., Kumar, P.S., Vo, D.-V.N. (2021). A review on the microbial degradation of chlorpyrifos and its metabolite TCP. Chemosphere, 283, 131447. https://doi.org/10.1016/j.chemosphere.2021.131447

[11] Bradford, M.M. (1976). A rapid and sensitive method for the quantitation of microgram quantities of protein utilizing the principle of protein-dye binding. Analytical Biochemistry, 72(1–2), 248–254. https://doi.org/10.1016/0003-2697(76)90527-3

[12] Chamnongpol, S., Willekens, H., Moeder, W., Langerbartels, C., Sandermann, H., Van Montagu, M., Inze, D., Van Camp, W. (1995). Defense activation and enhanced pathogen tolerance induced by H_2O_2 in transgenic tobacco. Molecular Plant-Microbe Interactions, 8(1), 15–22.

[13] Deeba, F., Pandey, V., Pandey, A.K. (2017). Metabolomics insights for plant bioremediation: biochemical responses under heavy metal stress. Frontiers in Plant Science, 8, 1816. https://doi.org/10.3389/fpls.2017.01816

[14] Fang, L., Shi, T., Chen, J., Wu, X., Zhang, L. (2021). Kinetics and catabolic pathway of chlorpyrifos biodegradation and hydrolysis in an immobilized Cupriavidus nantongensis X1T bacterial system. Science of the Total Environment, 752, 141820. https://doi.org/10.1016/j.scitotenv.2020.141820

[15] Gadd, G.M. (2010). Metals, minerals and microbes: geomicrobiology and bioremediation. Microbiology, 156(3), 609–643. https://doi.org/10.1099/mic.0.037143-0

[16] Gangola, S., Sharma, A., Bhatt, P., Khati, P., Chaudhary, P. (2018). Presence of esterase and laccase in Bacillus subtilis facilitates biodegradation and detoxification of cypermethrin. Scientific Reports, 8, 12755. https://doi.org/10.1038/s41598-018-31082-5

[17] Gupta, A., Singh, R., Kaur, M. (2024). Synergistic bioremediation using bacterial consortia from chronically polluted sites: a mini-review. Frontiers in Microbiology, 15, 1352789. https://doi.org/10.3389/fmicb.2024.1352789

[18] Haque, S., Singh, R., Farooqi, A., Kaur, L., Tripathi, V., Prasad, R. (2021). An overview of heavy metal pollution and microbiome-dependent remediation in the Indian subcontinent. Frontiers in Microbiology, 12, 667719. https://doi.org/10.3389/fmicb.2021.667719

[19] Kanehisa, M., Furumichi, M., Sato, Y., Kawashima, M., Ishiguro-Watanabe, M. (2023). KEGG for taxonomy-based analysis of pathways and genomes. Nucleic Acids Research, 51(D1), D587–D592. https://doi.org/10.1093/nar/gkac963

[20] Kumar, S., Stecher, G., Tamura, K. (2015). MEGA7: Molecular Evolutionary Genetics Analysis version 7.0 for bigger datasets. Molecular Biology and Evolution, 33(7), 1870–1874. https://doi.org/10.1093/molbev/msw054

[21] Li, Y., Qian, H., Liu, K., Tang, Y. (2025). Microbial communities in industrial soils under multi-metal stress: diversity, function and bioremediation prospects. Journal of Hazardous Materials, 461, 132672. https://doi.org/10.1016/j.jhazmat.2024.132672

[22] Mali, H., Shah, C., Patel, K.G., Trivedi, U.B., Bhavsar, P.S. (2022). Bioremediation of organophosphate pesticide chlorpyrifos in contaminated environments: a mechanistic review. Environmental Technology and Innovation, 27, 102412. https://doi.org/10.1016/j.eti.2022.102412

[23] Malwe, A.S., Bhushan, B., Murugesh, E., Sharma, N., Kaur, K., Vyas, A., Bhattacharya, B.K., Sinha, S. (2025). XenoBug: a database and comprehensive analysis of xenobiotic-transforming microbial enzymes. Applied Microbiology and Biotechnology, 109(1), 45. https://doi.org/10.1007/s00253-025-13397-2

[24] Megharaj, M., Ramakrishnan, B., Venkateswarlu, K., Sethunathan, N., Naidu, R. (2011). Bioremediation approaches for organic pollutants: a critical perspective. Environment International, 37(8), 1362–1375. https://doi.org/10.1016/j.envint.2011.06.003

[25] Ohkawa, H., Ohishi, N., Yagi, K. (1979). Assay for lipid peroxides in animal tissues by thiobarbituric acid reaction. Analytical Biochemistry, 95(2), 351–358. https://doi.org/10.1016/0003-2697(79)90738-3

[26] Pande, A., Pandey, S.C., Sati, D., Pande, V., Samant, M. (2022). Bioremediation of heavy metals through microbial processes. Environmental Science and Pollution Research, 29(33), 43983–44009. https://doi.org/10.1007/s11356-022-20602-6

[27] Pegu, G., Das, P., Saikia, U. (2025). Soil contamination in peri-urban India: sources, distribution and remediation strategies. Environmental Geochemistry and Health, 47(2), 68. https://doi.org/10.1007/s10653-025-02358-1

[28] Phogat, A., Singh, T., Prasad, R., Banerjee, A., Gohel, S., Kumari, S. (under review). Isolation, ICP-MS heavy metal removal and GC-MS pesticide residue reduction by Planomicrobium sp. A9, most closely related to P. okeanokoites NBRC 12536 (97.71% 16S rRNA similarity) from co-contaminated industrial soils of Haryana: companion study to the present work. [Journal name withheld for blind review].

[29] Saini, P., Raj, D., Gupta, V., Mujral, R.L., Punia, K. (2023). Planomicrobium sp. P4: a salt-tolerant PGPR mitigating drought stress in Vigna radiata. Frontiers in Plant Science, 14, 1170613. https://doi.org/10.3389/fpls.2023.1170613

[30] Singh, B.K., Walker, A. (2006). Microbial degradation of organophosphorus compounds. FEMS Microbiology Reviews, 30(3), 428–471. https://doi.org/10.1111/j.1574-6976.2006.00018.x

[31] Tietze, F. (1969). Enzymic method for quantitative determination of nanogram amounts of total and oxidized glutathione: applications to mammalian blood and other tissues. Analytical Biochemistry, 27(3), 502–522. https://doi.org/10.1016/0003-2697(69)90064-5

[32] Yarza, P., Yilmaz, P., Pruesse, E., Glöckner, F.O., Ludwig, W., Schleifer, K.-H., Whitman, W.B., Euzeby, J., Amann, R., Rosselló-Móra, R. (2014). Uniting the classification of cultured and uncultured bacteria and archaea using 16S rRNA gene sequences. Nature Reviews Microbiology, 12(9), 635–645. https://doi.org/10.1038/nrmicro3330

[33] Yoon, J.-H., Kang, K.-H., Park, Y.-H. (2001). Planomicrobium koreense gen. nov., sp. nov., a bacterium isolated from the Yellow Sea in Korea, and transfer of Planococcus okeanokoites (Nakagawa et al. 1996) to Planomicrobium sp. A9, most closely related to P. okeanokoites NBRC 12536 (97.71% 16S rRNA similarity) comb. nov. International Journal of Systematic and Evolutionary Microbiology, 51(4), 1511–1520. https://doi.org/10.1099/00207713-51-4-1511

[34] Zhang, H., Yuan, X., Xiong, T., Wang, H., Jiang, L. (2020). Bioremediation of co-contaminated soil with heavy metals and pesticides: influence factors, mechanisms and evaluation methods. Chemosphere, 247, 125923. https://doi.org/10.1016/j.chemosphere.2020.125923

[35] Zhou, X., Li, M., Yang, Y., Zhang, X., Chen, F. (2023). Microbial strategies for heavy metal removal in industrial wastewater: a comprehensive review. Journal of Cleaner Production, 414, 137553. https://doi.org/10.1016/j.jclepro.2023.137553